# Frictional forces in an electrolytic environment

L. I. Daikhin and M. Urbakh*
*School of Chemistry, Tel Aviv University, Ramat Aviv, Tel Aviv 69978, Israel*
(Received 6 July 1998)

We propose a theoretical description of frictional phenomena in nanoscale layers of electrolyte solutions embedded between two plates, one of which is externally driven. It is shown that the presence of nonuniform charge distributions on the plates leads to a space-dependent frictional force, which enters into the equation of motion for the top driven plate. The equation displays a rich spectrum of dynamical behaviors: periodic stick-slip, erratic, and intermittent motions, characterized by force fluctuations, and sliding above the critical velocity. Boundary lines separating different regimes of motion in a dynamical phase diagram are determined. The dependences of the frictional force and regimes of motion on an electrolyte concentration, a surface charge distribution, and a thickness of the liquid layer are predicted. The relevance to existing systems and predictions amenable to different experiments are discussed. [S1063-651X(99)01202-7]

PACS number(s): 68.45.−v, 68.15.+e, 47.27.Lx, 46.80.+j

## I. INTRODUCTION

Much attention has been recently developed within the field of nanotribology in the understanding of the nature of friction at a microscopic scale [1–4]. Sheared liquids confined between two atomically smooth solid surfaces provide a good example of a system where a broad range of phenomena and different behaviors have been experimentally observed [5–8]. These include dry frictionlike behavior observed for atomically thin liquid layers at low driving velocity, a transition to a liquidlike sliding with the increase of layer thickness and/or driving velocity, and shear thinning. These and other observations have motivated theoretical efforts, both numerical [9–15] and analytical [16–21], but many aspects of friction are still not well understood.

To get insights that will help establish the basics of nanotribology it is necessary to perform measurements under well defined conditions and to have a possibility to change interactions in a controlled way. An electrochemical environment can provide such conditions for nanotribological studies. Electrode surfaces immersed in electrolyte have well defined properties. Dissolution of surface groups leads to charging of these surfaces, resulting in electrostatic interactions between surfaces. All electrostatic interactions are known and well described [22]. There are many ways to change interactions in electrochemical systems without changing any other properties of the measurement, for instance, by varying the electrolyte concentration and composition. Moreover, for conducting surfaces the surface potential can be changed during measurements, which allows one to distinguish between different contributions to frictional forces. Friction measurements performed in an electrolytic environment [23–25] have already demonstrated interesting dependences of frictional dynamics on the electrolyte concentration and on liquid film thickness.

In this paper we propose a theoretical description of frictional phenomena in a thin layer of electrolyte solution confined between two plates. The dependences of the frictional force and regimes of motion on the electrolyte concentration, the surface charge distribution, and the thickness of the liquid layer are studied. The proposed model leads to the observed experimental behavior and to predictions that are amenable to experimental tests. Up to now the majority of surface force apparatus (SFA) measurements have been performed with atomically flat mica surfaces [5–8] and therefore we do not consider here the effect of roughness on frictional forces. The presence of surface roughness may lead to mechanisms of friction [26,27] that are different from those discussed above.

The paper is organized as follows. In Sec. II we define the model and calculate frictional forces between two plates. The Poisson-Boltzmann approach is used for the calculation of electrostatic interactions. In Sec. III we introduce the equation of motion. Different dynamical regimes are discussed and transition between them are analyzed. Section IV summarizes our results. The Appendix presents a stability analysis of the regimes of motion.

## II. ELECTROSTATIC INTERACTIONS

We consider two plates separated by a thin layer of an electrolyte solution. The top plate of mass $M$ is pulled by a linear spring with a force constant $K$ connected to a stage that moves with a velocity $V$ (see Fig. 1). When the plate surfaces are in contact with an electrolyte they become charged. This leads to electrostatic interactions between plates. The charging of surfaces in a liquid can come in two ways [22]: by the ionization or dissociation of surface groups

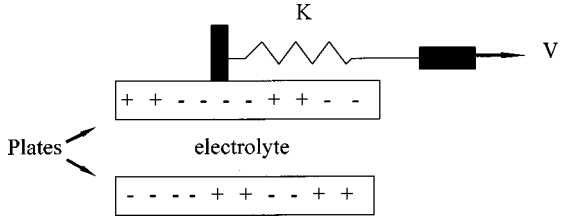


FIG. 1. Schematic sketch of a model geometry.

*Author to whom correspondence should be addressed. Electronic address: urbakh@post.tau.ac.il

 

or/and by the adsorption of ions from the solution. The charge on the solid surfaces is obviously not uniformly distributed over the surfaces. The discreteness of the surface charges is a natural source of this nonuniformity. The surface roughness may serve as an additional source of the charge nonuniformity. It should be noted that the surface charge distribution depends on the conductivity of the plates.

The motion of the nonuniformly charged top plate gives rise to a reorganization of the ionic distribution in the electrolyte solution, which results in a resistance force acting on the top plate. The relaxation time of the ionic system $\tau_D$ could be estimated as $\tau_D^{-1}=\kappa^2 D$ [28], where $\kappa^{-1}$ is the Debye length and $D$ is the diffusion coefficient of the ions in the solution. For a 1-1 binary electrolyte solution $\kappa^{-1}=(\epsilon_{\rm el}k_BT/8\pi ne^2)^{1/2}$, where $n$ is the electrolyte concentration, $\epsilon_{\rm el}$ the dielectric constant of the solvent, $e$ the charge of electron, $T$ the temperature, and $k_B$ the Boltzmann constant. In $0.1M-0.001M$ aqueous solutions $\tau_D^{-1}$ is typically $10^7-10^9\ {\rm s}^{-1}$. The characteristic time related to the motion of the nonuniform surface charge could be estimated as $\tau_m^{-1}=V_{\max}/l$, where $l$ is the average distance between charges on the plate surfaces and $V_{\max}$ is the maximal velocity of the top plate. The charges on real surfaces are typically 1–10 nm apart from each other on average [22] and $V_{\max}$ does not exceed $10^2 v$ (see below), where the velocity of the stage $v$ is typically $10^{-2}-1\ \mu$m/s. As a result, $\tau_m^{-1}$ falls in the range $10^2-10^5\ {\rm s}^{-1}$. Our estimations demonstrate that the relaxation of the ionic atmosphere is much faster than the motion of surface charges. In this case the ionic system is in equilibrium at all times and the lateral, frictional, force acting on the top plate $\mathbf{\Pi}$ is determined by the variation of the free energy of the ionic system $\mathcal{F}$,

$$\mathbf{\Pi}=-\frac{\partial \mathcal{F}}{\partial \mathbf{X}}, \tag{1}$$

where $\mathbf{X}$ is the lateral displacement of the top plate with respect to the bottom one and the axis $x$ is chosen to coincide with the direction of motion.

If the ions in the solution are treated as a dilute, ideal gas, the free energy of the electrolyte plasma can be written as [29]

$$\begin{aligned}\mathcal{F}=kT\int d^3\mathbf{r}\{&n_+(\mathbf{r})[\ln n_+(\mathbf{r})/n-1]\\&+n_-(\mathbf{r})[\ln n_-(\mathbf{r})/n-1]+2n\}\\&+\frac{\epsilon_{\rm el}}{8\pi}\int d^3\mathbf{r}\,\nabla\phi(\mathbf{r})\nabla\phi(\mathbf{r}).\end{aligned} \tag{2}$$

Here $\phi(\mathbf{r})$ is the electrostatic potential in the electrolyte and $n_+(\mathbf{r})$ and $n_-(\mathbf{r})$ are the concentrations of positive and negative ions, which are related to the potential by the equations

$$n_\pm(\mathbf{r})=n\exp[\mp e\phi(\mathbf{r})/k_BT]. \tag{3}$$

In order to calculate the force $\mathbf{\Pi}$, one needs the distribution of the electrostatic potential $\phi(\mathbf{r})$ in the electrolyte. The latter is described by the solution of the Poisson-Boltzmann equation [22,29]. As a first step we restrict our consideration by its linearized version, valid for low potentials $\phi<k_BT/e$:

$$(\nabla^2-\kappa^2)\phi(r)=0. \tag{4}$$

The solution of Eq. (4) must satisfy the boundary conditions relating the normal component of electrostatic displacement to the surface charge densities at the plates. We describe the surface charge densities at the bottom and the top plates by the functions $\sigma_0(\mathbf{R})$ and $\sigma_d(\mathbf{R}+\mathbf{X})$, respectively. The planes $z=0$ and $d$ are chosen to coincide with the plate surfaces and $\mathbf{R}=(x,y)$ denotes a tangential coordinate. Then the boundary conditions can be written as

$$\begin{aligned}\epsilon_{\rm el}\frac{\partial\phi(z=0+,\mathbf{R})}{\partial z}-\epsilon_{\rm sub}\frac{\partial\phi(z=0-,\mathbf{R})}{\partial z}&=4\pi\sigma_0(\mathbf{R}),\\ \epsilon_{\rm sub}\frac{\partial\phi(z=d+,\mathbf{R})}{\partial z}-\epsilon_{\rm el}\frac{\partial\phi(z=d-,\mathbf{R})}{\partial z}&=4\pi\sigma_d(\mathbf{R}+\mathbf{X}),\end{aligned} \tag{5}$$

where $\epsilon_{\rm sub}$ is the dielectric constant of the plates. A similar model, with uniform surface charge densities, has been used to study a normal pressure between two charged surfaces in an electrolyte solution [22,29].

Here we focus on the effect of lateral nonuniformity of the surface charge density, which plays an essential role in frictional phenomena. We assume that surface charge distributions $\sigma_0(\mathbf{R})$ and $\sigma_d(\mathbf{R}+\mathbf{X})$ are frozen and do not depend of the relative displacement of the plates. The influence of fluctuations of surface charges on the interactions between plates has been considered in Ref. [30].

In solving Eq. (4) it is convenient to Fourier transform the potential and the charge densities from the tangential coordinates $\mathbf{R}$ to the corresponding wave vectors $\mathbf{K}=(K_x,K_y)$ so that $f(\mathbf{K})=\int d\mathbf{R}\,f(\mathbf{R})\exp(-i\mathbf{K}\cdot\mathbf{R})$. Equation (1) then transforms to

$$\left\{\frac{d^2}{dz^2}-K^2-\kappa^2\right\}\phi(K,z)=0. \tag{6}$$

The solution of Eq. (6) in the layer $0<z<d$ has the form

$$\phi(z,\mathbf{K})=A(\mathbf{K})\exp(-q_Kz)+B(\mathbf{K})\exp(q_Kz), \tag{7}$$

where $q_K=\sqrt{\kappa^2+K^2}$. The boundary conditions in Eq. (5) lead to the equations for the prefactors $A(\mathbf{K})$ and $B(\mathbf{K})$,

$$\begin{aligned}A(\mathbf{K})=\frac{2\pi}{D(K)}\{&\sigma_0(\mathbf{K})(\epsilon_{\rm el}q_K+\epsilon_{\rm sub}K)\exp(q_Kd)\\&+\sigma_d(\mathbf{K})(\epsilon_{\rm el}q_K-\epsilon_{\rm sub}K)\exp(iK_xX)\},\\ B(\mathbf{K})=\frac{2\pi}{D(K)}\{&\sigma_0(\mathbf{K})(\epsilon_{\rm el}q_K-\epsilon_{\rm sub}K)\exp(-q_Kd)\\&+\sigma_d(\mathbf{K})(\epsilon_{\rm el}q_K+\epsilon_{\rm sub}K)\exp(iK_xX)\},\end{aligned} \tag{8}$$

where

$$D(K)=(\epsilon_{\rm el}^2q_K^2+\epsilon_{\rm sub}^2K^2)\sinh(q_Kd)+2\epsilon_{\rm el}\epsilon_{\rm sub}q_kK\cosh(q_Kd). \tag{9}$$

Then the distribution of the electrostatic potential in the solution has the form

$$\phi(\mathbf{R},z)=\int \frac{d^2\mathbf{K}}{(2\pi)^2}\frac{4\pi\exp(i\mathbf{K}\cdot\mathbf{R})}{D(K)} \times\{\sigma_0(\mathbf{K})[\epsilon_{\rm el}q_K\cosh q_K(z-d) -\epsilon_{\rm sub}K\sinh q_K(z-d)]+\sigma_d(\mathbf{K})\exp(iK_xX) \times[\epsilon_{\rm el}q_K\cosh q_Kz+\epsilon_{\rm sub}K\sinh q_Kz]\}. \quad (10)$$

In the range of low potentials one may expand ion concentrations $n_\pm(\mathbf{r})$ in $e\phi/k_BT$. Then considering terms up to the second order in $e\phi/k_BT$, Eq. (2) for the free energy reduces to

$$\mathcal{F}=\tfrac{1}{2}\int_{z=0}d^2\mathbf{R}\,\phi(\mathbf{R})\sigma_0(\mathbf{R})+\tfrac{1}{2}\int_{z=d}d^2\mathbf{R}\,\phi(\mathbf{R})\sigma_d(\mathbf{R}+\mathbf{X})$$
$$=2\pi\int\frac{d^2\mathbf{K}}{(2\pi)^2}\frac{1}{D(K)}\{[|\sigma_0(\mathbf{K})|^2+|\sigma_d(\mathbf{K})|^2] \times[\epsilon_{\rm el}q_K\cosh q_Kd+\epsilon_{\rm sub}K\sinh q_Kd] +2\sigma_d(\mathbf{K})\sigma_0(-\mathbf{K})\epsilon_{\rm el}q_K\exp(iK_xX)\}. \quad (11)$$

Substitution of Eq. (11) into Eq. (1) gives the final equation for the lateral force acting on the moving top plate

$$\Pi=4\pi i\int\frac{d^2\mathbf{K}}{(2\pi)^2}\frac{\epsilon_{\rm el}q_KK_x\sigma_d(\mathbf{K})\sigma_0(-\mathbf{K})\exp(iK_xX)}{D(K)}. \quad (12)$$

Equation (12) correlates the lateral force with the charge distributions on the plates. As an example, we assume periodically varying charge density distributions along the plate surfaces

$$\sigma_0(\mathbf{R})=\sigma_d(\mathbf{R})=\bar{\sigma}+\Delta\sigma\sin\frac{2\pi}{l}x. \quad (13)$$

This leads to the expression for the space-dependent lateral force

$$\Pi=b\sin\left(\frac{2\pi}{l}X\right), \quad (14)$$

where

$$b=\frac{4\pi^2(\Delta\sigma)^2S\epsilon_{\rm el}\sqrt{\kappa^2+(2\pi/l)^2}}{lD(K=2\pi/l)} \quad (15)$$

and $S$ is the area of the plate surfaces. Equation (15) can be simplified by taking into consideration that $\epsilon_{\rm el}\gg\epsilon_{\rm sub}$,

$$b=\frac{4\pi^2S(\Delta\sigma)^2}{\epsilon_{\rm el}l\sqrt{\kappa^2+(2\pi/l)^2}\sinh[d\sqrt{\kappa^2+(2\pi/l)^2}]}. \quad (16)$$

Equations (14)–(16) present the dependence of the frictional force on the distance between plates $d$, the electrolyte concentration $n$, and periodicity of the surface charge distributions $l$. The amplitude of the frictional force decreases exponentially with the distance between plates. In the range of high electrolyte concentrations $\kappa\geqslant 2\pi/l$, we predict a sharp decrease in $b$ as $n$ increases. For lower concentrations $\kappa<2\pi/l$, the amplitude $b$ depends only slightly on $n$.

Equation (12) applies also to a case of random charge distributions on the plates. It has been recently shown [31] that the presence of random charge distributions leads to a large number of minima in the energy of interaction between plates as a function of their relative parallel displacement. The typical energy associated with these minima scales as the square root of the plate area $S^{1/2}$ and for sufficiently large plates can be much larger than the thermal energy $k_BT$. The presence of such minima may lead to stick-slip phenomena for low driving velocities. Most dynamical behaviors found in the next section (stick-slip motion, transition to sliding, and so on) hold also for a random charge distribution.

## III. DYNAMICS OF FRICTION

The motion of the top driven plate, which is the basic observable in SFA experiments, is determined by the interplay between the electrostatic lateral force, a viscous friction, and the external spring force. Taking into consideration the separation of time scales, which correspond to the top plate motion and to the ionic subsystem relaxation, the dynamical equation for the plate can be written in the form

$$M\ddot{X}+\Gamma\dot{X}+K(X-Vt)-b\sin(2\pi X/l)=0. \quad (17)$$

The dissipative force $\Gamma\dot{X}$ in Eq. (17) describes the viscous friction at the top plate-solution interface $\Gamma=\eta_{\rm eff}S/d$, where $\eta_{\rm eff}$ is the effective viscosity in the confined liquid layer. The effective viscosity of the thin layer may differ essentially from the bulk viscosity of the solution [6].

The important outcome of our electrostatic consideration is that the effective frictional force $F_{\rm fr}=-\Gamma\dot{X}+b\sin(2\pi X/l)$ in the equation of motion for the macroscopic mechanical degrees of freedom [Eq. (17)] has to be space dependent as obtained in Eq. (14). The space dependence of the friction force reflects properties of the microscopic interactions at the surfaces, namely, the nonuniformity of the surface charge distribution at the plate surfaces taken here as periodic. The typical lateral length scale of the electrostatic interaction $l$ reappears in the macroscopic friction force. The independence of the lateral force $\Pi$ of the velocity is a consequence of the fact that the relaxation time of the embedded system $\tau_D$ is faster than the characteristic time related to the motion of the top plate $\tau_m$. Similar equations with space-dependent frictional forces emerge also in other systems, for instance, in the case of dry friction [20(b),32].

It is convenient to introduce dimensionless space and time coordinates $y=2\pi X/l$ and $\tau=t\omega$, where $\omega=(2\pi/l)^{1/2}\sqrt{b/M}$ is the frequency of the small oscillations of the top plate in the minima of the periodic potential $(l/2\pi)b\cos(2\pi/lX)$. Equation (17) can be rewritten then in a dimensionless form as

$$\ddot{y}+\gamma\dot{y}-\sin(y)+\alpha(y-v\tau)=0. \quad (18)$$

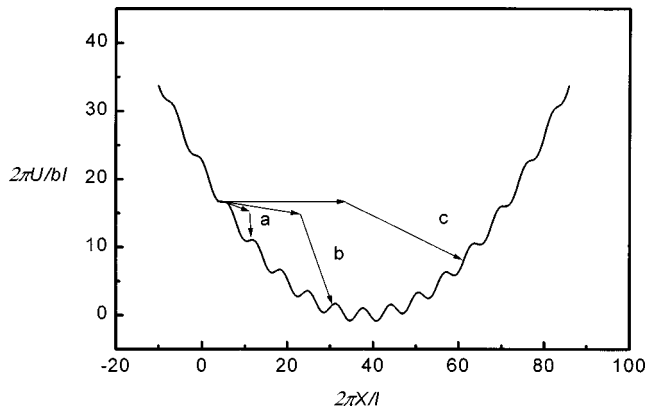


FIG. 2. Dimensionless total potential $2\pi U(X,t)/bl$ versus the dimensionless plate coordinate $2\pi X/l$ drawn for $\alpha=0.03$ and $v\tau=40$. Arrows indicate a slip motion (a jump) of the plate for three different dynamical regimes $a-c$ discussed in the text.

The dynamical behavior of the model is determined by the following dimensionless parameters: $\gamma=\Gamma/M\omega$ is a dimensionless dissipation constant, $\alpha=(\Omega/\omega)^2$ is the square of the ratio of the frequency of the free oscillations of the top plate $\Omega=\sqrt{K/M}$ to $\omega$, and $v=2\pi V/\omega l$ is the dimensionless stage velocity. The model leads to a number of different regimes of the motion of the top driven plate, which is the experimental observable. Below we discuss the dependence of the plate motion on the parameters of the system.

### A. Low-velocity regime

The main objective of the SFA experiments is to deduce information on microscopic properties of the system from the observed dynamics of the top plate. For this purpose one needs to understand the dependence of the dynamics on the mechanical (external) parameters and the parameters of the embedded system (internal). First we investigate the motion of the plate for very small velocities of the stage $v\ll 1$. In this case, the motion can involve two steps: slow motion (creep) in a local minima of the total potential $U(X,t)$ (see Fig. 2)

$$U(X,t)=\frac{l}{2\pi}b\cos\left(\frac{2\pi}{l}X\right)+\frac{K}{2}(X-Vt)^2 \qquad (19)$$

and a fast slip (sliding) that begins when an instability occurs, i.e., $d^2U/dX^2$ changes sign. The latter is possible for $\alpha<1$ only. At the point of instability the spring force reaches a maximum value corresponding to the static friction force $F_s$. The static friction equals the maximum value of the lateral force acting on the top plate, the amplitude $b$ in Eq. (14),

$$F_s=b. \qquad (20)$$

During a sliding the spring force $F=K(X-Vt)$ decreases until it reaches a value $F_k$ where the sliding ceases and the top plate is trapped again at a potential minima. Thus a periodic stick-slip motion of the top plate is observed for $v\ll 1$ and $\alpha<1$ [see Figs. 3(a)–3(c)]. This type of motion has been recently observed in the experiments performed in electrolyte solutions [25]. For $\alpha>1$ no instabilities occur, $d^2U/dX^2\neq 0$, and at all times the plate follows adiabatically

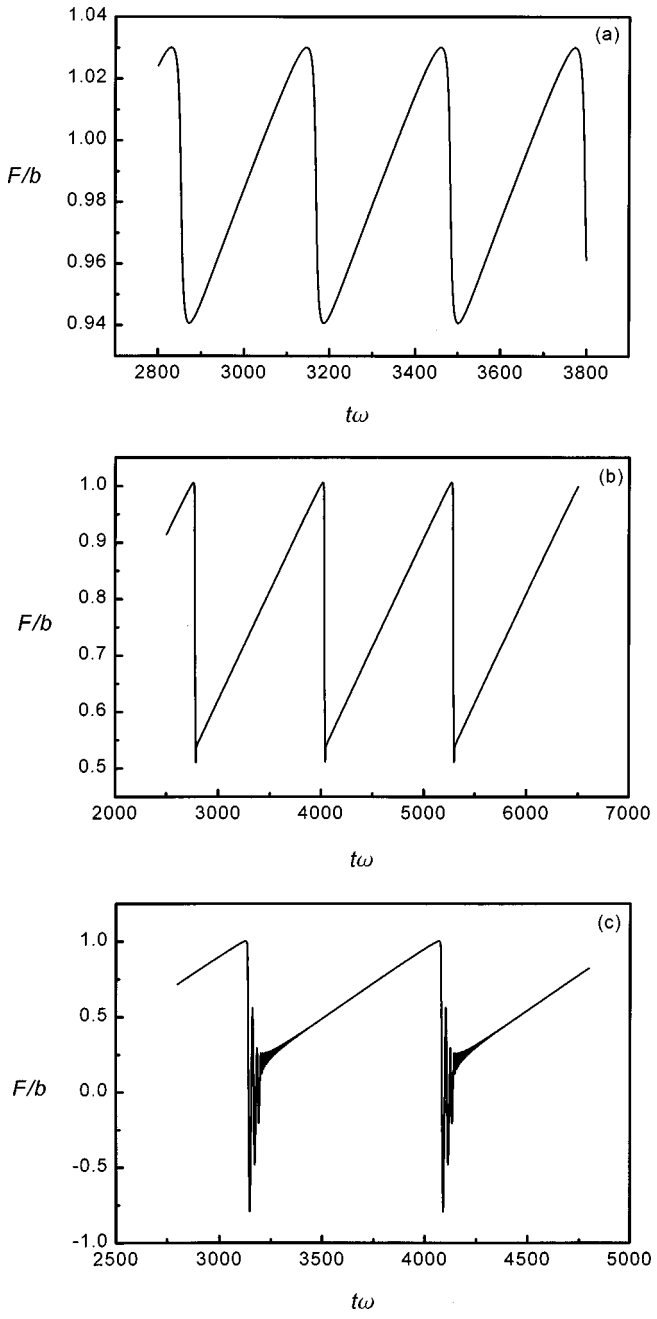


FIG. 3. Time series of the spring force $F$ for three regimes of the plate motion: (a) $\gamma=5$, $\alpha=0.02$, and $v=0.02$; (b) $\gamma=0.5$, $\alpha=0.02$, and $v=0.02$; and (c) $\gamma=0.03$, $\alpha=0.05$, and $v=0.02$. The spring force is presented in units of static frictional force $b$.

the motion of the stage being in a minima of the total potential. Here we concentrate on the dynamics of the system in the most interesting case of $\alpha<1$, when the electrostatic interaction between plates is stronger than the external spring force.

The dynamics of the stick-slip motion could be analyzed taking into account that the stage is effectively at rest during the fast slip of the plate $Vt=L_0=\text{const}$. The time pattern of the stick-slip motion is determined by the relationship between parameters $\alpha$ and $\gamma$. Three regimes can be distinguished [20(b)]: (a) $\gamma^2/4\gg 1$, where the system is overdamped [Fig. 3(a)]; (b) $\alpha<\gamma^2/4<1$, where the system is underdamped with respect to the periodic potential and over-

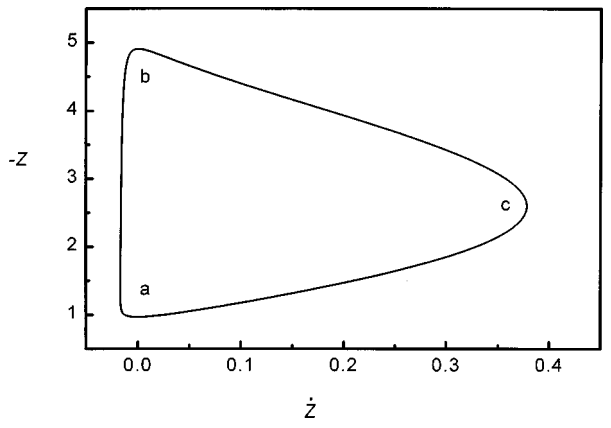


FIG. 4. Phase space representation of the plate motion in the overdamped regime for $\gamma=4$, $\alpha=0.2$, and $v=0.02$. $z$ and $\dot{z}$ are presented in dimensionless units.

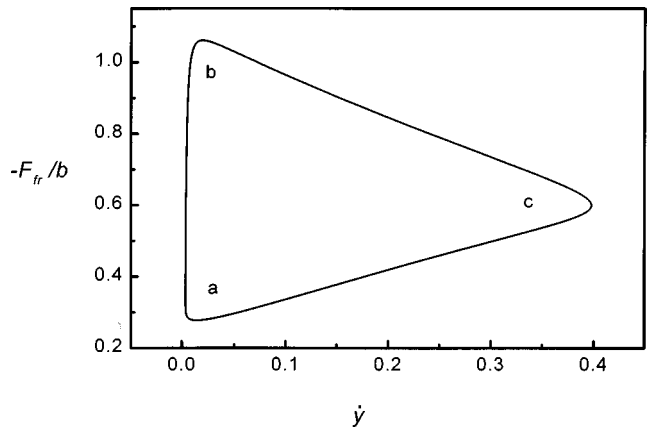


FIG. 5. Dimensionless frictional force $F_{\mathrm{fr}}/b$ versus the dimensionless velocity of the plate $\dot{y}$. The parameters are the same as in Fig. 4.

damped with respect to the driving spring [Fig. 3(b)]; and (c) $\gamma^2/4 \ll \alpha \ll 1$, where the system is underdamped [Fig. 3(c)].

*(a)* $\gamma^2/4 \gg 1$. In this regime the ''slip'' motion of the top plate corresponds to the jump between nearest-neighbor minima of the potential $U(X,t=L_0/V)$ and the slip distance $\Delta$ is about $l$, the period of the lateral force $\Pi$.

The energy dissipated during the slip is

$$\Delta W = U(X_0,L_0) - U(X_1,L_0). \tag{21}$$

Here $X_0$ and $L_0$ are the position of the plate and the length of the spring at the saddle point given by $dU/dX=0$ and $d^2U/dX^2=0$, where the slip starts, and $X_1$ is the next larger value of $X$ that satisfies $dU/dX=0$. The coordinates $X_0$ and $L_0$ are shown to be

$$X_0 = l\left(1 - \frac{1}{2\pi}\arccos(\alpha)\right), \tag{22}$$

$$L_0 = X_0 + \frac{l}{2\pi\alpha}(1-\alpha^2/2). \tag{23}$$

For low driving velocities the average friction force, which is defined as the dissipated energy per unit length, i.e., $\Phi = \Delta W/\Delta$, can be calculated analytically for two limiting cases [32]

$$\Phi = 9b(1-\alpha)^2/\pi + O((1-\alpha)^3) \quad \text{for } 0<1-\alpha\ll 1, \tag{24}$$

$$\Phi = b + O(\alpha) \quad \text{for } \alpha \ll 1. \tag{25}$$

The finite value of the frictional force found here for $v\to 0$ is a result of instabilities of the potential $U(X,t)$. Similar effects have been also found in other microscopic models of friction [12,20,32] and in large-scale molecular dynamics simulations [14].

Important information on the nature of stick-slip motion and on a transition to sliding could be obtained from a phase portrait ($z=y-v\tau+\gamma v/\alpha$ vs $\dot{z}=\dot{y}-v$), which characterizes the oscillatory motion of the system. The phase space representation is closely related to the dependence of the spring force $\alpha(v\tau-y)$ on the top plate velocity $\dot{y}$, which has been studied experimentally [33]. Figure 4 shows a representative phase portrait of the overdamped regime: $\alpha=0.2$, $\gamma=4$, and $v=0.02$. The interval $[a,b]$ corresponds to a very slow motion (creep) of the top plate located in the minima of the potential $U(X,t)$. The top plate starts to slide at the saddle point $b$ where the instability occurs, approaches the maximal velocity at the point $c$, and comes to rest at $a$.

We have also calculated an instantaneous frictional force $F_{\mathrm{fr}} = -\Gamma\dot{X} + b\sin(2\pi X/l)$ as a function of plate velocity (see Fig. 5). This quantity could be derived from the SFA experimental data [33,34] providing additional information on the frictional dynamics. During the creep period, $F_{\mathrm{fr}}$ increases linearly in time from $a$ to $b$. When $F_{\mathrm{fr}}$ reaches the static friction the top plate starts to slide. During the acceleration $(bc)$ $F_{\mathrm{fr}}$ decreases monotonically from $F_s$ as the velocity increases. During the deceleration $(ca)$ $F_{\mathrm{fr}}$ continues to decrease. Our calculations show that the frictional force is not a single-valued function of the velocity. A similar effect has been observed in a recent measurement of friction in granular materials [33]. The difference between Figs. 4 and 5 is caused by the contribution of the acceleration of the plate and becomes more pronounced for $\gamma<1$. A detailed analysis of a transition from stick-slip motion to sliding within the overdamped regime has been performed in Refs. [20(b), 32].

*(b)* $\alpha<\gamma^2/4<1$. In this regime the system manifests a qualitatively different dynamical behavior. Figure 6 presents phase portraits calculated for different values of the dimensionless spring constant $\alpha$. The following important features of the top plate motion should be noted. (i) The slip distance increases with the decrease of $\alpha$ and could be much larger than the period $l$. The number of maxima of $\dot{z}$ as a function of $z$, seen from the phase portrait, corresponds to a number of periods covered by the plate during the slip. (ii) After sliding, the plate oscillates while approaching the stable equilibrium position that corresponds to the focus. The equilibrium position itself moves in the direction of the next jump and the nature of the singular point ($\partial^2U/\partial X^2=0$) changes, transforming from the focus into the node and then into the saddle point.

In order to understand the dependence of the slip distance on $\alpha$ and $\gamma$ we have derived an approximate analytical expression for the top plate velocity $\dot{X}$ using the energy balance equation

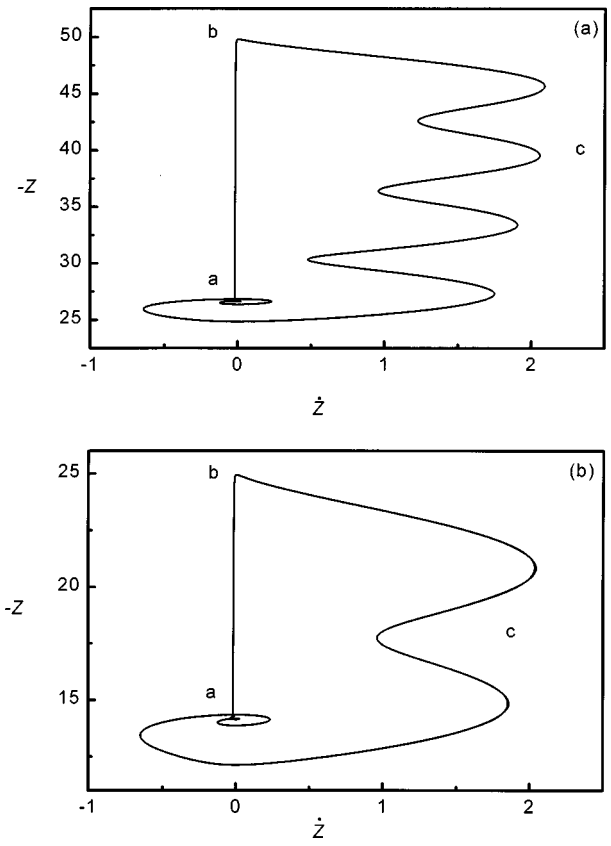


FIG. 6. Phase space representation of the plate motion for $\alpha < \gamma^2/4 < 1$: (a) $\gamma = 0.5$, $\alpha = 0.02$, and $v = 0.02$ and (b) $\gamma = 0.5$, $\alpha = 0.04$, and $v = 0.02$. $z$ and $\dot{z}$ are presented in dimensionless units.

$$\frac{M\dot{X}^2}{2} - \frac{l}{2\pi} b \cos\left(\frac{2\pi}{l} X\right) + \frac{K}{2}(X - L_0)^2 = U(X_0, L_0) - \Gamma \int_{X_0}^{X} \dot{X}\, dX. \tag{26}$$

Equation (26) has been solved using the expression for the dissipated energy, which was found by the solution of Eq. (17) in the zeroth order in $b$. This approximate solution of Eq. (26) is in good agreement with the results of numerical calculations of $\dot{X}(X)$ according Eq. (17). The slip distance $\Delta$ could be determined as a distance between the point $X = X_0$, where the slip starts, and the next turning point, where $\dot{X} = 0$. As a result, for $\alpha \ll 1$ we obtain

$$\Delta \approx \frac{l}{2\pi\alpha}\left[1 - \sqrt{2}\gamma\left(1 - \frac{g(\gamma)}{\gamma}\right)\right], \tag{27}$$

where

$$g(\gamma) = \sqrt{\pi} - \frac{3}{2\gamma} + \frac{\exp(-\sqrt{\pi}\gamma)}{2\gamma}[4 - \exp(-\sqrt{\pi}\gamma)]. \tag{28}$$

Equation (27) shows that the slip distance increases proportionally to $b/Kl$. Figure 7 shows the dependences of $\Delta$ on $\alpha$ for $\gamma = 0.5$.

The energy dissipated during the slip $\Delta W$ can be evaluated in a similar manner as was done in the overdamped regime. We find that for $\alpha \ll 1$, $\Delta W$ is proportional to the slip distance. As a result, the average friction force, which was defined as the dissipated energy per unit length, should be estimated with the help of Eqs. (24) and (25) derived above for $\Delta \approx l$.

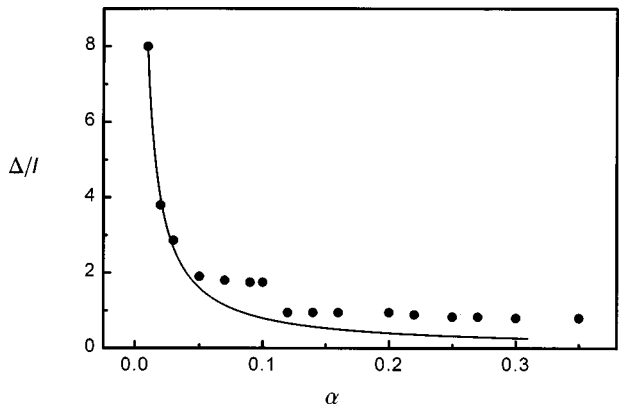


FIG. 7. Slip distance $\Delta$ versus the dimensionless spring constant $\alpha$. Closed circles show the results of numerical calculations and the solid line corresponds to calculations according to Eq. (27). $\Delta$ is presented in units of the period of surface charge distribution $l$. The dimensionless dissipation constant $\gamma = 0.5$ and $v = 0.02$.

Low driving velocity measurements help to distinguish between two fundamental quantities: static ($F_s$) and kinetic ($F_k$) friction forces. $F_s$ is the force needed to initiate the motion and $F_k$ is the minimal force necessary to keep the plate sliding. As we have already mentioned above, $F_s$ is expressed by the amplitude of the periodic lateral force [Eq. (20)]. When considering the kinetic friction, the dissipative nature of the system enters and $F_k$ depends also on $\Gamma$. For $a < \gamma^2/4 < 1$ the kinetic friction can be obtained by balancing the gain in energy due to driving force and the energy loss due to dissipation [35]. This argument leads to

$$F_k = \frac{4}{\pi}\gamma b. \tag{29}$$

In the regimes (a) and (b) discussed so far, the static and kinetic friction forces correspond to the maxima and minima in the spring force observed during stick-slip oscillations [see Figs. 3(a) and 3(b)] [5]. Figure 8 demonstrates that results of numerical calculations of $F_k$ follow Eq. (29).

Our calculations show that time patterns of the stick-slip motion depend on (i) the parameters of the embedded system (thickness of the liquid layer $d$, concentration of the electrolyte solution $n$, and lateral length scale $l$) and (ii) the mechanical parameters (mass of the top plate $M$ and spring constant $K$). All these parameters are included in the dimensionless quantities $\alpha$ and $\gamma$. In the case of the electrolyte solution confined between two plates the parameter $\alpha$ increases exponentially with the distance $d$ between plates and/or electrolyte concentration $n$ [see Eqs. (15) and (16)]. Thus the increase of $d$ and/or $n$, for given $K$, $M$, and $V$, should lead to a decrease in the sliding distance and to a transition from stick-slip motion to smooth sliding. These conclusions are in agreement with the preliminary experimental results [25].

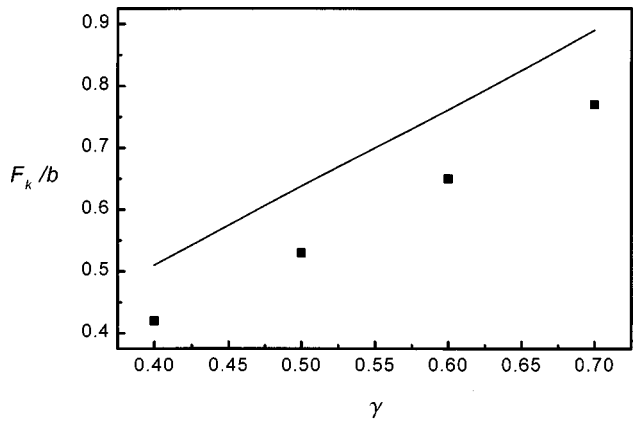


FIG. 8. Dependence of the kinetic frictional force $F_k$ on the dimensionless dissipation constant $\gamma$. Closed squares are results of numerical calculations and the solid line corresponds calculations according to Eq. (29). $F_k$ is presented in units of the static frictional force $b$. $\alpha=0.5$ and $v=0.02$.

*(c)* $\gamma^2/4 \ll \alpha \ll 1$. In this regime the periodic motion of the system includes a stick period followed by slowly attenuated oscillations [20(b)]. The top plate starts to slip from the saddle point, overshoots the lowest well of the total potential $U(X,L_0)$, and bounces a few times across the modulated parabola (see Fig. 2) before it slowly comes to rest into one of the pinning wells. This behavior is illustrated by the phase portrait presented in Fig. 9. It should be mentioned that the minimal spring force observed during stick-slip oscillations is negative and the amplitude of the oscillations is closed to $2F_s$.

### B. Transition from stick-slip motion to sliding

As the stage velocity increases the stick-slip motion of the top plate becomes more erratic and intermittent and then changes to periodically modulated sliding state. Figure 10 shows the dynamical phase diagram (in the $\alpha$-$v$ plane), which presents regions of parameters that correspond to different regimes of motion of the top plate. Stick-slip motion and smooth sliding occur, respectively, to the left of the solid line $v_c^{(1)}(\alpha)$ and to the right of the dashed line $v_c^{(2)}(\alpha)$. The system exhibits an intermittent motion in the range of parameters between these two curves. The lines $v_c^{(1)}(\alpha)$ and $v_c^{(2)}(\alpha)$ describe the $\alpha$ dependences of the critical velocities corresponding to transitions between different states of motion. They have been found by the analysis of numerical solutions of Eq. (17). The following characteristic features of the phase diagram should be mentioned.

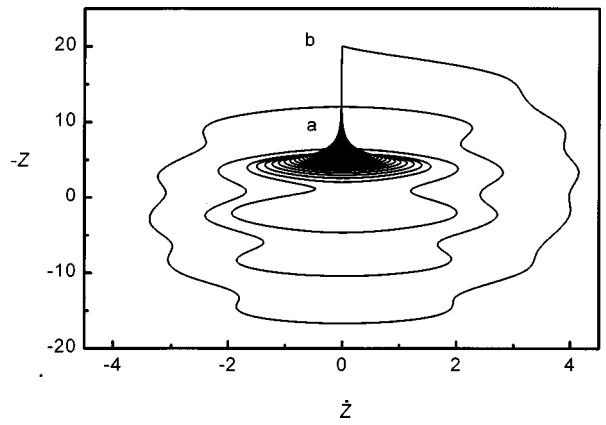


FIG. 9. Phase space representation of the plate motion in the underdamped regime for $\gamma=0.03$, $\alpha=0.05$, and $v=0.02$. $z$ and $\dot{z}$ are presented in dimensionless units.

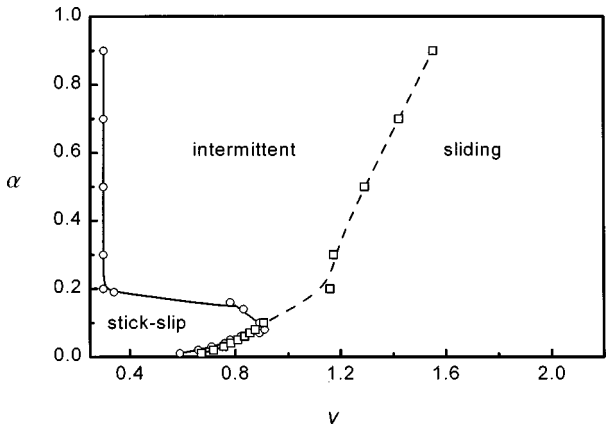


FIG. 10. Dynamical phase diagram for the plate motion. The solid line $v_c^{(1)}(\alpha)$ indicates the boundary between the stick-slip and intermittent motions and the dashed line $v_c^{(2)}(\alpha)$ is the lower velocity boundary of the smooth sliding. Open circles and squares show the results of numerical calculations of $v_c^{(1)}(\alpha)$ and $v_c^{(2)}(\alpha)$, respectively. The stage velocity $v$ and the spring constant $\alpha$ are presented in dimensionless units. The dimensionless dissipation constant $\gamma=0.5$.

(a) For $0.2<\alpha<1$ the critical velocity $v_c^{(1)}(\alpha)$ separating stick-slip from the intermittent motion depends only slightly on $\alpha$. Here the stick-slip motion corresponds to jumps between nearest-neighbor cells of the total potential $U$ (see Fig. 2). The analysis of the phase portrait shows that the stick-slip state holds as long as the relaxation of the top plate to the local minimum of the potential $U(X,t)$ after a slip event is faster than the motion of this minimum. As a result, the critical velocity $v_c^{(1)}(\alpha)$ increases with the increase of $\gamma$. It should be noted that in this range of parameters we observed a smooth transition from the stick-slip to intermittent motion and therefore the boundary line $v_c^{(1)}(\alpha)$ is not well defined here. Since for $0.2<\alpha<1$ the slip distance lies in a nanometric range $\Delta \approx l$, it should be hard to distinguish experimentally between this type of stick-slip motion and the periodically modulated sliding.

(b) With the decrease of $\alpha$ we observed a steep rise in the critical velocity $v_c^{(1)}(\alpha)$ that parallels the increase of the slip distance. The critical velocity as a function of $\alpha$ has a sharp maximum for $\alpha=\alpha_{\max}\approx 0.1$. For smaller values of $\alpha$, $\alpha<\alpha_{\max}$, two boundary lines $v_c^{(1)}(\alpha)$ and $v_c^{(2)}(\alpha)$ approach each other. Numerical calculations show that for all values of parameters the overdamped regime $\alpha<\gamma^2/4$ lies within the interval $\alpha<\alpha_{\max}$, where $v_c^{(1)}(\alpha)$ decreases with decrease of $\alpha$. For $\alpha<\alpha_{\max}$ the critical velocity $v_c^{(1)}(\alpha)$ decreases as $\gamma$ increases. As it has been already mentioned in [20(b)], for $\alpha<\alpha_{\max}$ the motion bifurcates discontinuously from a periodic stick-slip motion to an intermittent one.

The line $v_c^{(2)}(\alpha)$ separating the periodically modulated sliding from the intermittent motion could be found analytically by a linear stability analysis of the solutions of Eq. (18)

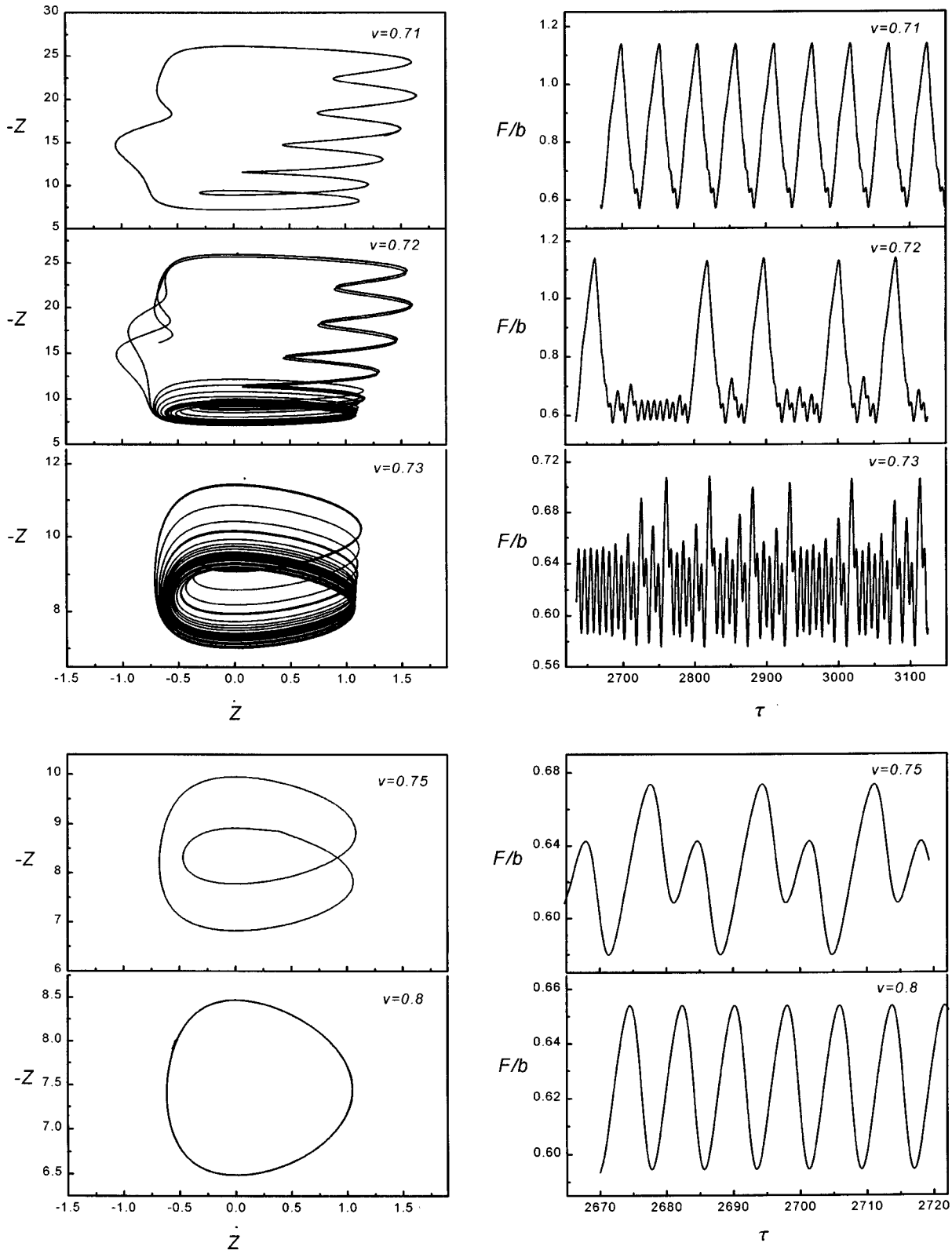


FIG. 11. Phase portraits and the time series of the spring force for different stage velocities. Stage velocities are denoted on the graphs. The spring force is presented in units of the static frictional force $b$. $\gamma=0.5$ and $\alpha=0.03$. $F$ is presented in units of the static frictional force $b$ and $z$ and $\dot{z}$ are presented in dimensionless units.

[18(b),18(c)]. For this purpose let us rewrite Eq. (18) in the form

$$\ddot{z}+\gamma\dot{z}+\alpha z+\sin(z)\cos(v\tau-v\gamma/\alpha)+\cos(z)\sin(v\tau-v\gamma/\alpha)=0, \tag{30}$$

where $z=y-v\tau+\gamma v/\alpha$. Equation (30) describes a damped harmonic oscillator that is driven parametrically by the external force $f=-\sin(z)\cos(v\tau)-\cos(z)\sin(v\tau)$. For high driving velocities $v\gg 1$ the solution of Eqs. (18) and (30) has the form of the periodically modulated sliding state [32]

$$y = v\tau + \gamma v/\alpha + \sin(v\tau)/v^2. \quad (31)$$

Besides the sliding state of Eq. (31), modulated with the frequency $v$ we observed also subharmonic oscillations with frequencies $v/n$ $(n=2,3,\ldots)$ that arise due to parametric resonances [18(b),18(c)]. Parametric resonance is an instability phenomenon. In the Appendix we find velocity intervals that correspond to these instabilities. For $\gamma \approx 1$ the system exhibits the first-order $(n=2)$ paramentric resonance only. The critical velocity $v_c^{(2)}(\alpha)$ is defined as the largest driving velocity at which the first-order parametric resonance is able to destabilize the sliding state (31). This condition yields the equation (see the Appendix)

$$v_c^{(2)}(\alpha) = 2\{\alpha - \gamma^2/2 + \tfrac{1}{2}\sqrt{\gamma^4 - 4\gamma^2\alpha + 1}\}^{1/2}, \quad (32)$$

which approximates well the numerical solution $v_c^{(2)}(\alpha)$ presented in Fig. 10. When the driving velocity decreases and becomes lower than $v_c^{(2)}(\alpha)$ the period of the top plate oscillations is doubled and their amplitude increases sharply. For a low dissipation constant $\gamma \ll 1$ we also observe an instability corresponding to the $n$th-order parametric resonances, with $n>2$. These resonances could exist for velocities $v > v_c^{(2)}(\alpha)$ (see the Appendix). The period of top plate oscillations equals $2\pi n/v$ in the vicinity of the resonances.

As the driving velocity varies from $v_c^{(1)}(\alpha)$ to $v_c^{(2)}(\alpha)$ the motion of the top plate bifurcates from the periodic stick-slip motion to modulated sliding. Above $v_c^{(1)}(\alpha)$ the stick-slip motion becomes erratic and intermittent. For a wide range of system parameters we find that the motion is chaotic. Figure 11 shows various examples of phase portraits and time series of the spring force as one passes from the stick-slip motion to sliding. The amplitude and the period of force oscillations decrease drastically as the driving velocity increases. The results presented have been calculated for the case of $\alpha \ll 1$ when the slip distance is much larger than the period of the plate potential. The system exhibits a rich spectrum of behaviors within the interval $[v_c^{(1)}(\alpha), v_c^{(2)}(\alpha)]$ even though it is very narrow for chosen parameters. This makes it clear that the transition from the periodic stick-slip motion to smooth sliding cannot be characterized by a single critical velocity (a single boundary line). The dynamical phase diagram should include two boundary lines $v_c^{(1)}(\alpha)$ and $v_c^{(2)}(\alpha)$ in order to account for the region of the intermittent motion, which is essential for the understanding of the frictional dynamics.

## IV. CONCLUSIONS

We have proposed a theoretical description of frictional phenomena in nanoscale layers of electrolyte solutions. It has been shown that the presence of nonuniform charge distributions on the plates gives rise to a space-dependent frictional force. This force depends strongly on the distance between plates $d$, electrolyte concentration $n$, and the lateral length scale of the surface charge distributions $l$. A separation of time scales for the plate motion and the relaxation of the ionic subsystem allowed us to derive the equation of motion (17) that includes only one, macroscopic degree of freedom, the displacement of the top driven plate. The microscopic properties of the system enter this equation through the frictional force derived above. The equation leads to a spectrum of behaviors in the motion of the plate: periodic stick-slip, erratic, and intermittent motions, characterized by force fluctuations, and sliding above the critical velocity $v_c^{(2)}(\alpha)$. For a given driving velocity the dynamical properties of the system are determined by two dimensionless parameters: $\alpha = Kl/2\pi b$, the ratio of the spring force for the stretching $l$ to the amplitude of the lateral electrostatic interaction between plates, and $\gamma = \Gamma/(2\pi b M/l)^{1/2}$, the dissipation constant. Measurements in a electrolytic environment make it possible to change these parameters in a controlled way by varying the electrolyte composition and concentration and the distance between plates [see Eqs. (15) and (16)]. For conducting surfaces the surface charge densities $\sigma_0$ and $\sigma_d$ could be easily changed, which will strongly influence the parameter $\alpha$. We have shown that the increase of $d$ and/or $n$ should result in a decrease of the amplitude of stick-slip oscillations and the slip distance and in the transition from the stick-slip to intermittent motion and to smooth sliding. These conclusions are in agreement with the preliminary results of experimental measurements in aqueous solutions [25]. Our calculations also demonstrated that a variation of the electrolyte concentration and the distance between plates strongly affects the dynamical phase diagram [leads to a shift of the boundary lines $v_c^{(1)}(\alpha)$ and $v_c^{(2)}(\alpha)$], which could be determined experimentally [36].

Although in this work we analyzed the case of the periodic charge distribution, similar dynamical phenomena should occur also for a random charge distribution. However, contrary to the results discussed above, for a random charge distribution the stick-slip motion can be erratic even for very low driving velocities. The elucidation of relationships between the time patterns of the spring force and the surface charge distribution is in progress. The erratic stick-slip motion may also have its origin in the roughness of the plate surfaces [26,27]. However, we believe that further investigations of the regimes of motion and the dynamical phase diagram as a function of the electrolyte concentration and the distance between plates will allow one to distinguish between the effect of the electrostatic interactions discussed here and the effect of surface roughness.

Our theoretical consideration shows that experiments performed in an electrolytic environment can provide deeper insight into the mechanism of frictional phenomena in nanoscale confined liquids. We hope that the present work will stimulate further experimental studies of friction under electrochemical conditions.

## ACKNOWLEDGMENTS

The authors thank J. Klafter for a critical reading of the manuscript and useful comments and C. Caroli, F.-J. Elmer, P. Graf, S. Granick, J. Klein, A. Nitzan, and S. Safran for discussions. Financial support for this work by the Israel Science Foundation and DIP grants is gratefully acknowledged.

## APPENDIX

Here we consider a subharmonic response of the system on the external force $f = -\sin(z)\cos(v\tau) - \cos(z)\sin(v\tau)$. We

use the standard theory of the parametric resonance [37], i.e., we look for the solutions of Eq. (30) that have the form

$$z = z_0 + A\sin(\omega\tau + \psi). \tag{A1}$$

Here $\omega = v/n$ and $n = 2,3,\ldots$ . The substitution of Eq. (A1) into Eq. (30) leads to the equations for $z_0$ and $A$

$$z_0 = -0.5\frac{\gamma}{\alpha}\omega A^2\frac{1}{n}, \tag{A2}$$

$$(\alpha - \omega^2)^2 + \gamma^2\omega^2 b_n(A) - a_n(A) = 0, \tag{A3}$$

where

$$b_n(A) = \frac{[J_{n-1}(A) - J_{n+1}(A)]^2}{[J_{n-1}(A) + J_{n+1}(A)]^2}, \tag{A4}$$

$$a_n(A) = \frac{[J_{n-1}(A) - J_{n+1}(A)]^2}{A}, \tag{A5}$$

and $J_n(A)$ are the Bessel functions of the order $n$. When deriving Eqs. (A2) and (A3) we have used the Bessel function expansions [38] of functions $\sin[\sin(x)]$ and $\cos[\sin(x)]$ and conserved constants and terms oscillating with the frequency $\omega$ only. It is convenient to rewrite Eq. (A3) in the form

$$\omega^2 = \alpha - 0.5\gamma^2 b_n(A) \pm \{0.25\gamma^4 b_n^2(A) - \gamma^2\alpha b_n(A) + a_n(A)\}^{1/2}. \tag{A6}$$

The solutions of Eqs. (A2) and (A3) exist in the interval of frequencies

$$\omega_n^{(\min)} < \omega < \omega_n^{(\max)}, \tag{A7}$$

where

$$\omega_n^{(\min)} = (\alpha - h_n^{(\min)})^{1/2}, \quad \omega_n^{(\max)} = (\alpha + h_n^{(\max)})^{1/2} \tag{A8}$$

and

$$h_n^{(\max)} = \max_A\{-0.5\gamma^2 b_n(A) + [0.25\gamma^4 b_n^2(A) - \alpha\gamma^2 b_n(A) + a_n(A)]^{1/2}\}, \tag{A9}$$

$$h_n^{(\min)} = \max_A\{0.5\gamma^2 b_n(A) + [0.25\gamma^4 b_n^2(A) - \alpha\gamma^2 b_n(A) + a_n(A)]^{1/2}\}. \tag{A10}$$

The values $h_n^{(\max)}$ and $h_n^{(\min)}$ should be real and the conditions $\alpha + h_n^{(\max)} > 0$ and $\alpha - h_n^{(\min)} > 0$ should be fulfilled. Then the amplitude $A$ and the shift $z_0$ are determined by Eqs. (A2) and (A3) for a given value of $\omega$ lying in the range from $\omega_n^{(\min)}$ to $\omega_n^{(\max)}$.

For $n = 2$ the maximum and minimum frequencies $\omega_1^{(\min)}$ and $\omega_1^{(\max)}$, are reached for $a_2 = 0.25$ and $b_2 = 1$ and we obtain the expressions for velocities.

$$v_2^{(\max)} = 2\omega_2^{(\max)} = 2\{\alpha - 0.25\gamma^2 + (\gamma^4 - 4\alpha\gamma^2 + 1)^{1/2}\}^{1/2}, \tag{A11}$$
$$v_2^{(\min)} = 2\omega_2^{(\min)} = 2\{\alpha - 0.25\gamma^2 - (\gamma^4 - 4\alpha\gamma^2 + 1)^{1/2}\}^{1/2},$$

bounding the interval where the solution (A1) exists. The analysis of Eq. (A6) shows that for $\gamma \geqslant 1$ there is only one interval $[v_2^{(\min)}, v_2^{(\max)}]$ where subharmonic behavior is observed. For $\gamma \ll 1$ the intervals corresponding to $n > 1$ are also allowed. It should be noted that for all values of the parameters $\alpha$ and $\gamma$ there is only a finite number of intervals where solutions (A1) could exist. The numerical calculations confirm the above conclusions.


[1] *Fundamentals of Friction*, Vol. 220 of *NATO Advanced Study Institute, Series E: Applied Sciences*, edited by I. L. Singer and H. M. Pollock (Kluwer Academic, Dordrecht, 1992).

[2] B. Bhushan, J. N. Israelachvili, and U. Landman, Nature (London) **374**, 607 (1995).

[3] *Micro/Nanotribology and Its Applications*, Vol. 330 of *NATO Advanced Study Institute, Series E: Applied Sciences*, edited by B. Bhushan (Kluwer Academic, Dordrecht, 1997).

[4] B. N. J. Persson, *Sliding Friction. Physical Principles and Applications* (Springer-Verlag, Berlin, 1998).

[5] H. Yoshizawa, P. McGuiggan, and J. Israelachvili, Science **259**, 1305 (1993); H. Yoshizawa, Y. L. Chen, and J. Israelaclivili, J. Phys. Chem. **97**, 4128 (1993); A. D. Berman, W. A. Ducker, and J. N. Israelaclivili, Langmuir **12**, 4559 (1996).

[6] H.-W. Hu, G. A. Carson, and S. Granick, Phys. Rev. Lett. **66**, 2758 (1991); G. Reiter, A. L. Demirel, and S. Granick, Science **259**, 1305 (1993); A. L. Demirel and S. Granick, Phys. Rev. Lett. **77**, 4330 (1996).

[7] J. Klein and E. Kumacheva, Science **269**, 816 (1995); J. Chem. Phys. **108**, 996 (1998); E. Kumacheva and J. Klein, *ibid.* **108**, 7010 (1998).

[8] J. M. Georges, A. Tonck, and J. L. Loubet, J. Phys. II **6**, 57 (1996); J. Crassous, E. Charlaix, and J. L. Loubet, Phys. Rev. Lett. **78**, 2425 (1997).

[9] P. A. Thompson and M. O. Robbins, Science **250**, 792 (1990); P. A. Thompson, M. O. Robbins, and G. S. Grest, Isr. J. Chem. **35**, 93 (1995).

[10] J. P. Gao, W. D. Luedtke, and U. Landman, Science **270**, 605 (1995); U. Landman, W. D. Luedtke, and J. P. Gao, Langmuir **12**, 4514 (1996); J. P. Gao, W. D. Luedtke, and U. Landman, Phys. Rev. Lett. **79**, 705 (1997).

[11] B. N. J. Persson, Phys. Rev. Lett. **71**, 1212 (1993); Phys. Rev. B **51**, 13 568 (1995); B. N. J. Persson and A. Nitzan, Surf. Sci. **367**, 261 (1996).

[12] M. G. Rozman, M. Urbakh, and J. Klafter, Phys. Rev. E **54**, 6485 (1996); **54**, 6485 (1996); Europhys. Lett. **39**, 183 (1997).

[13] O. Braun, T. Dauxois, and M. Peyrard, Phys. Rev. B **56**, 4987 (1997).

[14] Ph. Bordarier, M. Schoen, and A. H. Fuchs, Phys. Rev. E **57**, 1621 (1998).

[15] J. Roder, J. E. Hammerberg, B. L. Holian, and A. R. Bishop, Phys. Rev. B **57**, 2759 (1998).

[16] J. M. Carlson and A. A. Batista, Phys. Rev. E **53**, 4153 (1996).
[17] M. Urbakh, L. Daikhin, and J. Klafter, Phys. Rev. E **51**, 2137 (1995); Europhys. Lett. **33**, 125 (1995); J. Chem. Phys. **103**, 10 707 (1995).
[18] (a) F.-J. Elmer, J. Phys. A **30**, 6057 (1997); (b) M. Weiss and F.-J. Elmer, Z. Phys. B **104**, 55 (1997); (c) T. Strunz and F.-J. Elmer, Phys. Rev. E **58**, 1601 (1998).
[19] Y. Braiman, F. Family, and G. Hentschel, Phys. Rev. B **55**, 5491 (1996).
[20] (a) T. Baumberger, C. Caroli, B. Perrin, and O. Ronsin, Phys. Rev. E **51**, 4005 (1995); (b) T. Baumberger and C. Caroli, Eur. Phys. J. B **4**, 13 (1998).
[21] J. B. Sokoloff, Phys. Rev. B **42**, 760 (1990); **52**, 7205 (1995).
[22] J. N. Israelachvili, *Intermolecular and Surface Forces*, 2nd ed. (Academic, London, 1991).
[23] A. Dhinojwala and S. Granick, J. Am. Chem. Soc. **119**, 241 (1997).
[24] E. Weiland, B. Zink, Th. Stifter, and O. Marti, in *Micro/Nanotribology and Its Applications* (Ref. [3]), p. 283.
[25] M. Wilhelm and J. Klein (private communication).
[26] L. Daikhin and M. Urbakh, Phys. Rev. E **49**, 1424 (1994).
[27] T. Baumberger and C. Caroli, MRS Bull. **23**, 41 (1998).
[28] P. Delahey, *Double Layer and Electrode Kinetics* (Wiley, New York, 1966).
[29] S. A. Safran, *Statistical Thermodynamics of Surfaces, Interfaces and Membranes* (Addison-Wesley, Reading, MA, 1994).
[30] P. A. Pincus and S. A. Safran, Europhys. Lett. **42**, 103 (1998).
[31] S. Panyukov and Y. Rabin, Phys. Rev. E **56**, 7053 (1997).
[32] J. S. Helman, W. Baltensperger, and J. A. Holyst, Phys. Rev. B **49**, 3831 (1994).
[33] S. Nasuno, A. Kudrolli, and J. Gollub, Phys. Rev. Lett. **79**, 949 (1997).
[34] M. G. Rozman, M. Urbakh, J. Klafter, and F.-J. Elmer, J. Phys. Chem. **102**, 7924 (1998).
[35] H. Risken, *The Fokker-Planck Equation* (Springer, Berlin, 1984).
[36] T. Baumberger, F. Heslot, and B. Perrin, Nature (London) **367**, 544 (1994).
[37] L. D. Landau and E. M. Lifshitz, *Mechanics*, 3rd ed. (Pergamon, Oxford, 1976), Sec. 26.
[38] *Handbook of Mathematical Functions*, edited by M. Abramowitz and I. A. Stegen (Dover, New York, 1965).